An Optimization Approach to Teleoperation of the Thumb of a Humanoid Robot Hand: Kinematic Mapping and Calibration

Lei Cui[1]
Department of Mechanical Engineering,
Curtin University,
Kent Street,
Bentley, Western Australia 6102, Australia
e-mail: lei.cui@curtin.edu.au

Ugo Cupcic
Shadow Robot Company,
251 Liverpool Road,
London N1 1LX, UK
e-mail: ugo@shadowrobot.com

Jian S. Dai
Centre for Robotics Research,
King's College London,
University of London,
Strand, London WC2R 2LS, UK
e-mail: jian.dai@kcl.ac.uk

The complex kinematic structure of a human thumb makes it difficult to capture and control the thumb motions. A further complication is that mapping the fingertip position alone leads to inadequate grasping postures for current robotic hands, many of which are equipped with tactile sensors on the volar side of the fingers. This paper aimed to use a data glove as the input device to teleoperate the thumb of a humanoid robotic hand. An experiment protocol was developed with only minimum hardware involved to compensate for the differences in kinematic structures between a robotic hand and a human hand. A nonlinear constrained-optimization formulation was proposed to map and calibrate the motion of a human thumb to that of a robotic thumb by minimizing the maximum errors (minimax algorithms) of fingertip position while subject to the constraint of the normals of the surfaces of the thumb and the index fingertips within a friction cone. The proposed approach could be extended to other teleoperation applications, where the master and slave devices differ in kinematic structure. [DOI: 10.1115/1.4027759]

1 Introduction

Teleoperation permits the operation of machines at a distance, and it has been an integrated part of mechanical systems since 1950s, when Goertz built the first mechanical master-slave end-effector for manipulating radioactive materials [1].

Teleoperation finds applications in surgery, advanced manufacturing, and education. In surgery, teleoperation is exemplified in minimally invasive surgical robots [2–4], which enhance a surgeon's accuracy, dexterity, and visualization [5]. In advanced manufacturing, teleoperation allows human workers and robots to work intelligently together to combine human perceptual and problem-solving capabilities with the power and accuracy of machines [6]. In education, teleoperation enhances remote-learning by enabling students to access a robotics laboratory via the internet, overcoming the common problem institutions face: the limited availability of expensive robotics and control equipment, and thus provides a cost-effective way for students to acquire valuable "hand-on" experience [7–10].

A teleoperation interface consists of master and slave devices. The master device may be a keyboard or joystick [11], or haptic devices, such as data gloves and exoskeleton devices [12]. The slave device may be a physical robot or a computer generated representation of robots in a virtual world [8,10].

One impediment encountered in teleoperation is that the workspaces of master and slave devices differ intuitively and geometrically. System designers are obliged to develop mapping functions from the workspace of the master device to that of the slave device. Since exact mapping functions do not generally exist, designers adopt various optimization methods, which are widely used in mechanical design, including determination of the boundary of manipulator workspace [13], maximization of the dexterous regular workspace [14], optimization of joint stiffness of robotic arms [15], and design of the spherical serial manipulators [16].

The humanoid robotic hand is an example of slave device, whose real-time control poses substantial challenges, especially regarding the thumb motion. Studies [17–21] have shown that a rigid palm limits the dexterity of a robotic hand and an improved design furnishes the palm with extra degrees of freedom (DOFs), leading to a complex kinematic structure of the thumb.

The master devices for a humanoid robotic hand include parallel mechanisms [22,23], data gloves [24], and exoskeleton devices [12], where the latter two devices gain popularity in recent years due to intuitive user experience.

Exoskeleton master devices adopt the kinematic structure that imitates a human hand, such as the multifingered force-reflecting haptic device for grasp teleoperation [12]. Except for the thumb, the mapping is straightforward, since the hand mounted mechanism is capable of representing the joint angles. The operator needs to calibrate by extending and retracting one's fingers, allowing the program to record the minimum and maximum voltage signal delivered by potentiometers. The finger bend angles are calculated in a linear manner depending on the voltage readings.

It presents a substantial challenge to design an exoskeleton device for the thumb, for a planar linkage cannot capture the thumb position. One solution is a transverse pivotal mounting at the hand attachment point to account for the nonplanar motion of the thumb, but its effectiveness has not been reported [12].

Data-glove master devices use a human hand model to calibrate the joint sensor readings and map the hand motion to a robot for virtual manipulation or teleoperation [25–29]. While virtual manipulation calibration focuses on a visually acceptable representation of the human hand, teleoperation requires more accurate calibration and mapping. The use of data gloves does not alleviate the difficulties of teleoperating the thumb. Even with the aid of computer vision, some studies adopt optimization techniques to

[1]Corresponding author.

Contributed by the Mechanisms and Robotics Committee of ASME for publication in the Journal of Mechanical Design. Manuscript received October 26, 2013; final manuscript received May 19, 2014; published online June 13, 2014. Assoc. Editor: Matthew B. Parkinson.

estimate the centre of rotation from multiple surface markers on the thumb [30,31].

Several studies calibrate data gloves without using computer vision. After admitting the unfeasibility of simulating the whole thumb, each one of the studies concentrates on a different aspect. One study focuses on the thumb-tip point [28]; another study uses teleoperation for a planar two-fingered gripper—the thumb is overly simplified to a two DOFs planar series-chain [26]; a third study does not provide details about controlling the thumb motion, but mentions the advantages of teleoperation: the combination of the durability of a robot and the flexibility of a human mind to quickly develop and test control strategies [32].

Mapping the kinematic chains from a human hand to a robot hand could occur either in joint space or Cartesian space. Mapping in the joint space makes the hand poses look similar, an important factor for power grasps. Scale mismatch, i.e., differences in dimensions between the master and the slave devices, is another scenario where joint-space mapping is preferred, but this usually entails similar kinematic structures.

Mapping in the Cartesian space allows manipulating an object by the fingertips and is fit for objects that are graspable by a human hand. In literature, this is normally called a precision grasp, a pinch grasp, or a tip grasp [33–37]. Many humanoid robotic hands, including the Shadow Hand, are meant to replicate the functionality of a human hand and as a result, the dimensions of these hands are very close to a human hand. For example, the average length of a human hand measured from wrist to middle fingertip is 208.78 mm ($n = 80$) [38]; the length of the Shadow Hand from wrist to middle fingertip is 238.78 mm [39]. As to the thumb, the average total length of a human thumb is 137.5 mm ($n = 11$) [40]; the total length of the Shadow thumb is 106 mm. The difference between thumb lengths is alleviated by the difference of the whole hand lengths. For this reason, we adopted the mapping in the Cartesian space and focused on grasping the objects that are graspable by a human hand.

The paper is organized as follows. It first describes the setup of the hardware and compares a human-thumb workspace with a robot-thumb workspace. After proposing the mapping method that considers correlated sensor readings, it presents the experimental protocol involving only nine rigid objects of different lengths. The calibration is then formulated as minimizing the worst-case value of the set of grasping postures with the performance metrics and experimental results.

2 The Glove-Based Teleoperation

We demonstrated the proposed approach with a data glove—CyberGlove II [41]—and a humanoid robotic hand—Shadow Dexterous Hand.

Two factors complicate the implementation. First, the kinematic structure of a human thumb differs from that of a robotic thumb. On the one hand, the axes of the interphalangeal joint (IJ), the metacarpophalangeal joint (MPJ), and the trapeziometacarpal joint of a human thumb are not orthogonal or intersecting, as in Fig. 1. Thus, a kinematic chain with five orthogonal and intersecting axes of rotation cannot describe realistic thumb motion [40]. On the other hand, it is economically unfeasible for a robotic thumb to totally imitate the structure of a human thumb. This leads to five orthogonal axes for most robotic thumbs (including the Shadow Hand), endeavoring to duplicate a human-thumb motion.

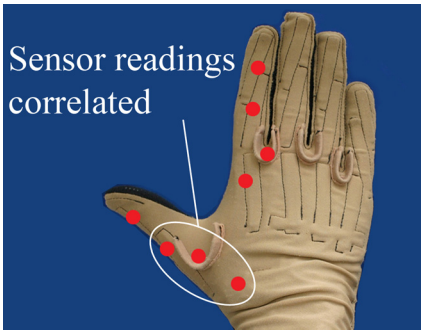

Fig. 2 The sensor positioning of the CyberGlove II

Second, data gloves are incapable of measuring all the independent thumb movements. For example, the CyberGlove II only measures four DOFs of the thumb motion and the sensor readings of rotation and abduction are correlated, as in Fig. 2.

Each joint of the CyberGlove II has two calibration parameters: gain and offset. The sensor strip at each joint gives the raw data reading and the glove's interface software converts this digital value into an angle using a calibration procedure. The users take a sequence of given poses, from which the gains and offsets are computed. The results are visually acceptable, representing a human hand across a wide variety of users. However, the spatial accuracy produced by the default calibration is not accurate enough for precision grasp.

Previous literature mainly focuses on calibrating and mapping fingertip positions, because most robotic hands then had hemispherical fingertips and generally no sensing capacity at the fingertips. Recently, an increasing number of humanoid robotic hands (including the Shadow Robot Hand) have the volar side soft-padded and equipped with tactile sensor and the distal side covered with fingernail. This renders the previous approaches inadequate—unnatural precision grasp may be generated, as in Fig. 3, where the thumb nail grasps the object.

Mapping and calibrating both the position and orientation of a human thumb, we proposed a novel nonlinear optimization formulation that minimizes the worst cases of positioning errors while subject to the normals of the thumb and index-finger surfaces within a friction cone.

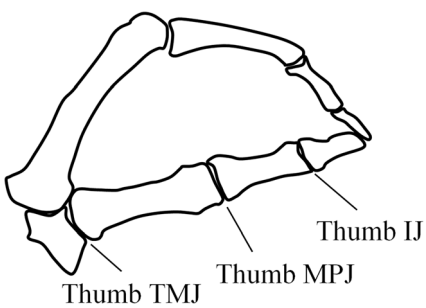

Fig. 1 Human-thumb joints

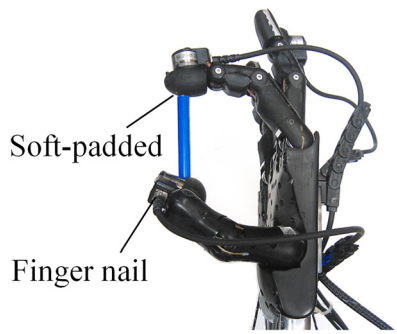

Fig. 3 Inadequate precision grasp due to calibrating fingertip position alone

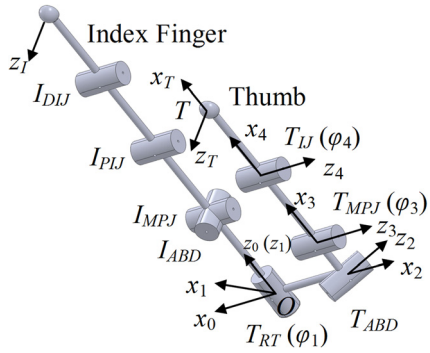

Fig. 4 The thumb model matching the sensor positioning of the CyberGlove II

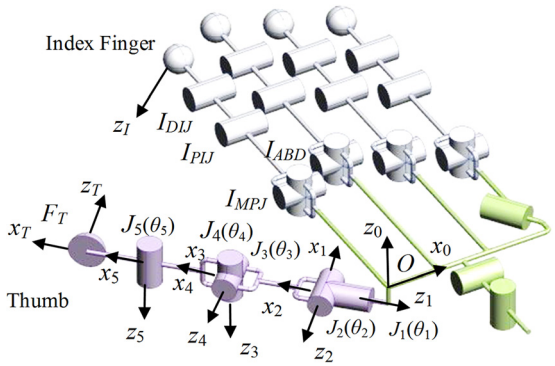

Fig. 6 The kinematic model of the thumb of the Shadow Hand

Table 1 The D–H parameters of the human-thumb kinematical model

	d_i (mm)	φ_i (rad)	a_i (mm)	δ_i (rad)
$T_0 - T_{RT}$	0	$\pi/2$	0	0
$T_{RT} - T_{AB}$	0	$[0, \pi/2]$	13.6	$3\pi/2$
$T_{AB} - T_{MPJ}$	0	$[-\pi/2, 0]$	52.9	$3\pi/2$
$T_{MPJ} - T_{IJ}$	0	$[0, \pi/2]$	40.3	0
$T_{IJ} - T_{Tip}$	0	$[0, \pi/2]$	30.7	$3\pi/2$

Table 2 The D–H parameters of the thumb of the shadow hand

	d_i (mm)	φ_i (rad)	a_i (mm)	δ_i (rad)
$T_0 - J_1$	29	$\pi/2$	8.5	$3\pi/4$
$J_1 - J_2$	0	$[-1.04, 1.04]$	0	$\pi/2$
$J_2 - J_3$	0	$[-1.40, 0]$	38.0	0
$J_3 - J_4$	0	$[-0.70, 0.70]$	0	$\pi/2$
$J_4 - J_5$	0	$[-0.26, 0.26]$	32	0
$J_5 - T_{Tip}$	0	$[0, \pi/2]$	27.5	$3\pi/2$

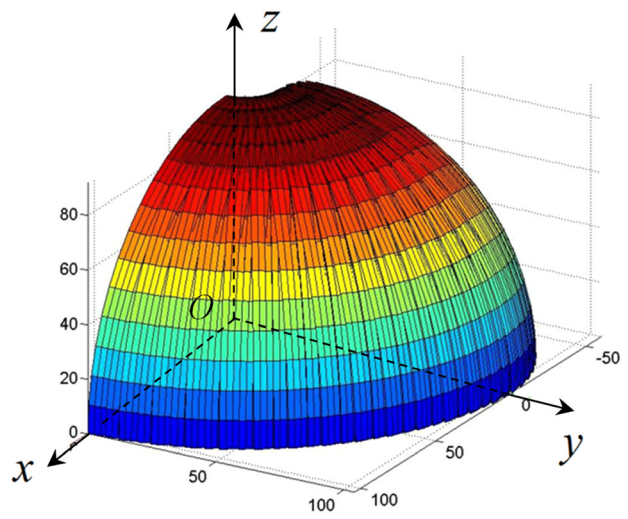

Fig. 5 The thumb-tip workspace of the human-thumb model

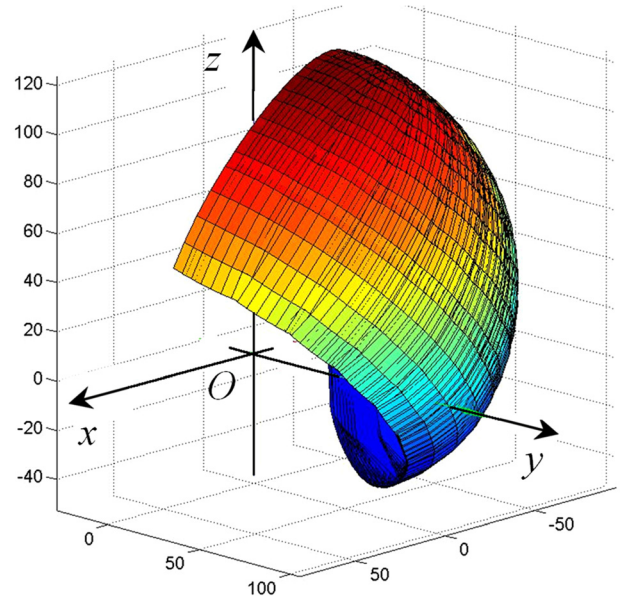

Fig. 7 The thumb-tip workspace of the Shadow Hand

3 Workspace Comparison of a Human Thumb and a Robot Thumb

A human thumb has a very complex kinematic structure [35,42], which hinders its model in a kinematic chain consisting of orthogonal revolute joints. We proposed a new thumb model that matches the sensor positioning of the CyberGlove II, as in Fig. 4, where T_{RT} represents thumb rotation, T_{ABD} thumb abduction, T_{MPJ} thumb MPJ, and T_{IJ} thumb IJ, and T the thumb-tip frame.

Denavit–Hartenberg (D–H) notation is the standard approach in robotics to describe joint kinematics for computational applications [43]. The global frame T_0 (O-$x_0y_0z_0$) was established in such a way that z_0 is along the T_{RT} axis and x_0 is along the common perpendicular line of T_{RT} axis and T_{AB} axis, as in Fig. 4. The phalange lengths of a human thumb come from the mean values of measurements of cadaveric thumbs ($n = 11$) [40], as in Table 1.

Forward kinematics yields the set of reachable thumb-tip positions—the workspace of the human-thumb model, as in Fig. 5.

The Shadow Hand thumb has five DOFs, with the global frame O-$x_0y_0z_0$ fixed to the palm body and O-$x_iy_iz_i$ fixed to each axis, as in Fig. 6.

The D–H parameters of the Shadow thumb are listed in Table 2 and the thumb-tip workspace of the Shadow Hand is shown in Fig. 7.

The two workspaces shown in Figs. 5 and 7 differ geometrically. Further the Shadow thumb has 1 more DOF than that of the human model, disallowing mapping the whole workspace linearly from the human thumb to the Shadow Hand thumb.

Hence, we considered only the part of the workspaces related to grasping by the thumb and the index finger and used linear

mapping to scale and skew the workspace of the human thumb to that of the robotic thumb.

4 Kinematic Mapping From the Human Thumb to the Robotic Thumb

We made two assumptions in the proposed kinematic mapping. The first was that the correlation of sensor readings can be modelled by linearly correlated gain coefficients; the second was that the joint angles of a human thumb can be linearly mapped to those of a robotic thumb.

Two parameters—gain and offset—generate the joint angles for each independent joint of the CyberGlove II

$$\varphi_i = g_i \beta_i - \varphi_i^0 \tag{1}$$

where φ_i the joint angle of the human hand, g_i the gain, β_i the sensor reading, and φ_i^0 the angle offset.

The independence of the T_{ij} sensor reading allows using the Eq. (1) directly to generate its angle

$$\varphi_4 = g_4 \beta_4 - \varphi_4^0 \tag{2}$$

However, the sensor readings of T_{RT}, T_{ABD}, and T_{MPJ} are correlated. We modeled this correlation by adding correlated gain coefficients as

$$\begin{bmatrix} \varphi_1 \\ \varphi_2 \\ \varphi_3 \end{bmatrix} = \begin{bmatrix} g_1 & g_1^{12} & g_1^{13} \\ g_2^{21} & g_2 & g_2^{23} \\ g_3^{31} & g_3^{32} & g_3 \end{bmatrix} \begin{bmatrix} \beta_1 \\ \beta_2 \\ \beta_3 \end{bmatrix} - \begin{bmatrix} \varphi_1^0 \\ \varphi_2^0 \\ \varphi_3^0 \end{bmatrix} \tag{3}$$

where φ_i is the joint angle, β_i is the sensor reading, φ_i^0 the offset, g_i the gain, and g_i^{jk} the correlated gain.

The first two joints of the human thumb and the robotic thumb—T_{IJ} and J_5, T_{MPJ} and J_4—have similar kinematic structure. Thus, the two angles of the human thumb can be mapped to those of the robotic thumb by multiplying a scalar factor k_i as

$$\begin{bmatrix} \theta_4 \\ \theta_5 \end{bmatrix} = \begin{bmatrix} k_1 & 0 \\ 0 & k_2 \end{bmatrix} \begin{bmatrix} \varphi_3 \\ \varphi_4 \end{bmatrix} \tag{4}$$

where θ_4 and θ_5 represent the joint angles of J_4 and J_5 of the Shadow thumb, respectively. Substituting Eq. (2) and the third linear equation in Eq. (3) into the above equation and merging the constants yield

$$\begin{bmatrix} \theta_4 \\ \theta_5 \end{bmatrix} = \begin{bmatrix} k_1 & 0 \\ 0 & k_2 \end{bmatrix} \left(\begin{bmatrix} g_3^{31} & g_3^{32} & g_3 & 0 \\ 0 & 0 & 0 & g_4 \end{bmatrix} \begin{bmatrix} \beta_1 \\ \beta_2 \\ \beta_3 \\ \beta_4 \end{bmatrix} - \begin{bmatrix} \varphi_3^0 \\ \varphi_4^0 \end{bmatrix} \right) \tag{5}$$

The angles θ_1, θ_2, and θ_3 of the Shadow Hand have to be generated from the two angles of the T_{RT} and T_{AB} joints. A 3×2 matrix containing scalar factors k_{ij} maps linearly from φ_1 and φ_2 to these three angles

$$\begin{bmatrix} \theta_1 \\ \theta_2 \\ \theta_3 \end{bmatrix} = \begin{bmatrix} k_{11} & k_{12} \\ k_{21} & k_{22} \\ k_{31} & k_{32} \end{bmatrix} \begin{bmatrix} \varphi_1 \\ \varphi_2 \end{bmatrix} \tag{6}$$

Substituting the first two linear equations of Eq. (3) into the above equation yields

$$\begin{bmatrix} \theta_1 \\ \theta_2 \\ \theta_3 \end{bmatrix} = \begin{bmatrix} k_{11} & k_{12} \\ k_{21} & k_{22} \\ k_{31} & k_{12} \end{bmatrix} \left(\begin{bmatrix} g_1 & g_1^{12} & g_1^{13} \\ g_2^{21} & g_2 & g_2^{23} \end{bmatrix} \begin{bmatrix} \beta_1 \\ \beta_2 \\ \beta_3 \end{bmatrix} - \begin{bmatrix} \varphi_1^0 \\ \varphi_2^0 \end{bmatrix} \right) \tag{7}$$

Combining Eqs. (5) and (7) into one linear equation and rewriting the coefficients give

$$\boldsymbol{\theta} = \mathbf{G}\boldsymbol{\beta} - \boldsymbol{\varphi}^{\mathbf{0}} \tag{8}$$

where

$$\boldsymbol{\theta} = \begin{bmatrix} \theta_1 \\ \theta_2 \\ \theta_3 \\ \theta_4 \\ \theta_5 \end{bmatrix}, \quad \boldsymbol{\beta} = \begin{bmatrix} \beta_1 \\ \beta_2 \\ \beta_3 \\ \beta_4 \end{bmatrix}, \quad \boldsymbol{\varphi}^0 = \begin{bmatrix} k_{11}\varphi_1^0 + k_{12}\varphi_2^0 \\ k_{21}\varphi_1^0 + k_{22}\varphi_2^0 \\ k_{31}\varphi_1^0 + k_{32}\varphi_2^0 \\ k_1\varphi_3^0 \\ k_2\varphi_4^0 \end{bmatrix}$$

$$\mathbf{G} = \begin{bmatrix} k_{11}g_1 + k_{12}g_2^{12} & k_{11}g_1^{12} + k_{12}g_2 & k_{11}g_1^{13} + k_{12}g_2^{23} & 0 \\ k_{21}g_1 + k_{22}g_2^{12} & k_{21}g_1^{12} + k_{22}g_2 & k_{21}g_1^{13} + k_{22}g_2^{23} & 0 \\ k_{31}g_1 + k_{32}g_2^{12} & k_{31}g_1^{12} + k_{32}g_2 & k_{31}g_1^{13} + k_{32}g_2^{23} & 0 \\ k_1 g_3^{31} & k_1 g_3^{32} & k_1 g_3 & 0 \\ 0 & 0 & 0 & k_2 g_4 \end{bmatrix}$$

The left side of the above equation gives the joint angles of the robotic thumb and the right side gives the mapping from the sensor readings β_i. This completes mapping the sensor readings of the human thumb to the joint angles of the robotic thumb.

The map function in Eq. (8) contains 22 parameters: k_i, g_i, k_{ij}, g_i^{jk}, and φ_i^0. Optimization in this dimension would have been computationally heavy; but scrutinizing it reveals a simpler form

$$\begin{bmatrix} \theta_1 \\ \theta_2 \\ \theta_3 \\ \theta_4 \\ \theta_5 \end{bmatrix} = \begin{bmatrix} a_{11} & a_{11} & a_{13} & 0 \\ a_{21} & a_{22} & a_{23} & 0 \\ a_{31} & a_{32} & a_{33} & 0 \\ a_{41} & a_{42} & a_{43} & 0 \\ 0 & 0 & 0 & a_{55} \end{bmatrix} \left(\begin{bmatrix} \beta_1 \\ \beta_2 \\ \beta_3 \\ \beta_4 \end{bmatrix} - \begin{bmatrix} b_1 \\ b_2 \\ b_3 \\ b_4 \end{bmatrix} \right) \tag{9}$$

This reduces the number of parameters from 22 to 17: a_{ij} and b_i, simplifying the optimization substantially. Empirical studies show that on a laptop with the Intel® *i*5 duo-core central processing unit and four gigabytes memory, the average optimization time is 8 min with the 17-parameter model and 14 min with the 22-parameter model.

5 Calibrating the Sensor Readings

5.1 A Minimum Extra-Hardware Experimental Protocol Without Computer Vision. We designed an experimental protocol that does not require computer vision. Admittedly, computer vision would have provided a redundant set of data to help compensate for the imprecision of data-glove measurements. However, the initial setup of computer-vision system—3D computer vision in this case—requires knowledge and experience in computer-vision hardware and software; especially when the computer-vision system would have to capture the small-scale movement of the thumb, and it thus involves high-resolution camera and accurate calibration—this would be time-consuming and expensive. A computer-vision system would also compromise the portability of the teleoperation system: the stereo camera would have to be supported to a proper height and proper lightening conditions would have to be provided.

This proposed experimental protocol involves only minimum extra hardware: a set of nine rigid objects of lengths from 10 mm to 90 mm. Each operator uses the precision grasp to grasp each of the nine rigid objects between the volar sides of the thumb and index fingertips with natural poses, as in Fig. 8.

In the select setup, the lengths of the rigid objects cover the graspable range by the index and thumb fingertips of a human hand, ensuring that the objects of intermediate length are also graspable.

Fig. 8 Generating sensor readings

5.2 Distance Optimization Subject to Surface-Normal Constraints. We assumed an antipodal grasp of a planar object with a friction-cone-contact model and a normal force large enough to provide the necessary momentum in the tangential and normal directions.

Recent robotic fingertips imitate a human fingertip with tactile sensors equipped on the volar side and fingernails on the distal side. It is thus important for precision grasps to keep the thumb and index fingers' volar sides facing each other and the two normal vectors within a friction cone [44].

Two contact models, frictional point contact and soft contact, have been used in studying grasping and manipulation in previous literature. The former is modelled by "friction cone" defined by the Coulomb friction, which determines the ratio of tangential to normal forces that can sustained without slipping [45]. The latter is established on the well-known Hertzian contact model, which assumes that linear elastic objects with small deformation [46,47]. Though the soft contact model is more realistic, it has to consider the geometry and forces of the contact surfaces. At issue is getting an accurate contact force in the tangential direction. Mechanics literature also recognizes it to be a difficult problem [48,49].

Adopting the friction-cone-contact model, we aimed to propose a general approach to teleoperation, for considering geometry and force of a particular hand would hinder its application to a variety of humanoid robotic hands.

Two metrics could be used to measure the performance of a thumb. The first one is given by the method of least squares, which evaluates the overall solution and minimizes the sum of the squares of the errors of the nine grasp set. This metric does not adequately address the problem because large deviation of one set could lead to the failure of precision grasp of a particular length. The second metric minimizes the maximum error (minimax algorithms) of the set of nine grasps as a worst-case problem, excelling in limiting the maximum deviation of all grasps.

Choosing the second metric, we casted the problem into a constrained nonlinear optimization: The algorithms generate the optimal parameters a_{ij} and b_i from the sensor readings of the experimental setup, where users grasp a set of nine rigid objects whose lengths span the distances between the two fingertips.

The readings of the index finger give the position and the orientation of the index fingertip, from which the desired position and the orientation of the thumb fingertip can be generated as

$$\begin{aligned} &\mathbf{F}_{Ti} = \mathbf{F}_{Ii} + L_i \mathbf{z}_{Ii} \\ &\frac{2\pi}{3} \le \psi_i \le \pi \end{aligned} \tag{10}$$

where $\boldsymbol{F}_{Ti}$ is the desired position vector the thumb fingertip, $\boldsymbol{F}_{Ii}$ is the position vector of the index fingertip, L_i the length of the rigid object, $\mathbf{z}_{Ii}$ the unit normal of the index fingertip surface, ψ_i is the angle of the normals of the tip surfaces, and i is the ith object grasped by the operator.

The first equation in Eq. (10) defines the distance requirement and the second equation defines that the normals of the two surfaces lie within the friction cone. The static friction coefficient between rubber and other materials could be in the range of 0.5–1, giving the friction-cone angle from 0.46 to 0.78. Thus, the angle ψ_i between these two fingertip normals is constrained between 120 deg and 180 deg with antipodal point grasps.

The mapping is formulated as an optimization problem as

$$\begin{aligned} &\min_x \max_i |\Delta d_i| \\ &\text{s.t.} -1 \le \mathbf{z}_{Ti} \cdot \mathbf{z}_{Ii} \le -\frac{1}{2} \end{aligned} \tag{11}$$

Δd_i is the difference between the desired thumb fingertip and the actual position and the dot product of the normals gives the normal constraint. The optimization variables are the 17 parameters a_{ij} and b_i in Eq. (9).

6 Validation and Results

The proposed method was tested on empirical studies. The method was implemented using MATLAB 7.1 (Mathworks, Inc.) and used the MATLAB *fminimax* function to minimize the worst-case value of the nine set of readings with the initial values obtained following the CyberGlove II User's manual and the constrained terms processed by a penalty function.

Sensor readings were recorded using a CyberGlove II, connected to a personal computer (PC) via serial port. The system recorded the sensor readings at the rate of 20 Hz for 10 readings—the mean values of each of the 10 readings were used. The resolution of each joint of CyberGlove II is approximately ±1 deg, sensor repeatability approximately ±3 deg, sensor linearity 0.6% maximum nonlinearity over full joint range. A Shadow Hand E1M3R was used, operating at a frequency of 1.0 Hz with a position control strategy in the host PC. The resolution of each joint is 0.2 deg.

Six able-bodied subjects took part in the study, hand length from fingertip to wrist 204.2 mm ± 8.7 mm (mean ± std, $n = 6$). Each subject was instructed to put on a data glove and fix it tightly at the wrist. Each subject then grasped the nine rigid objects (10 mm–90 mm) using natural poses, and sensor readings were generated and recorded on a PC. After calibration, each subject was instructed to teleoperate the Shadow Hand by grasping three objects of different lengths 25 mm, 50 mm and 75 mm, as in Fig. 9. The distances and normal vectors of the Shadow Hand at each test were recorded.

The empirical results are listed in Table 3, where the mean distance with its standard deviation and the mean normal angle with its standard deviation were obtained when the subjects telegrasped the objects of length 25 mm, 50 mm, and 75 mm, respectively.

7 Discussions

Two factors affected the calibration results. The first was that the resolution of each joint of CyberGlove II is approximately ±1 deg, which limits the grasping precision to no better than

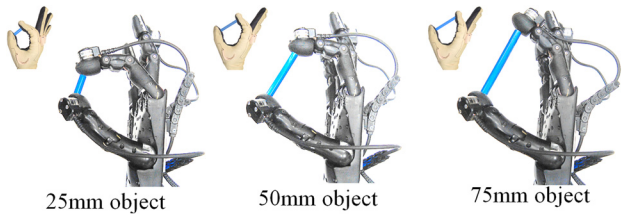

Fig. 9 Precision grasps of objects of length 25 mm, 50 mm, and 75 mm

Table 3 Empirical study results

Object length (mm)	Mean distance ± std (mm)	Mean angle ± std (deg)
25	22.3 ± 3.2	168.7 ± 18.3
50	43.1 ± 6.7	157.4 ± 11.2
75	70.5 ± 7.8	145.5 ± 10.6

1 mm in hand configurations. The second was that the precision grasp with the thumb and the index finger causes tip deformation. The maximum distance differences were estimated at 3 mm.

There are two main contributions of this work compared with previous work [25,26,28,50,51]. The first is, we presented a new kinematic model of the human thumb. One major difference between this model and previous one is that the MPJ joint in this work is perpendicular to the metacarpal bone, instead of being parallel to it [26]. This arrangement matches the glove-sensor positioning and is able to effectively measure the movement of the trapezium-metacarpal joint, while previous model measures the twist motion of this bone—current data gloves are not capable of this task. The proposed new model may provide new clues to develop a better exoskeleton device.

The second contribution is, we used a new metric, which minimizes the worst case of the range graspable by a human hand, while previous approaches minimize the overall performance in the sense of least squares. It has been shown that for any bounded parameter set, a minimax estimator achieves lower mean-squared error than the least-squares estimator over the entire parameter set [52,53]. Physically, it means that while the least-squares metric evaluates the overall performance, it fails to prevent large deviation occurring. The minimax metric considers the performance across the graspable range and yields better results.

We mapped the workspace in the Cartesian space. One issue of the approach is the slave device can only grasp objects that are graspable by a human hand. Extending the current mapping to larger objects would entail new experimental protocols: At issue is the mapping of the fingertip distances. One possible approach is via virtual grasp, where the setup sees a virtual hand that matches the size of the robotic hand and the kinematic structure of a human hand. Another possible approach is to equip the robotic hand with proximity sensing, such as tactile sensors, and equip the data glove with physical stimulus device, such as vibration motor. The proximity sensing triggers the vibration motor, closing the loop and giving the users the sense of distance.

Mapping in the joint space would have solved the problem of scale mismatch and enabled the robotic hands grasp larger objects. However, one impediment exists: the structure mismatch. The human thumb and the robot thumb differ in terms of structure and DOFs. For example, the Shadow thumb has five DOFs, while the CyberGlove II can only measure four DOFs of a human thumb. This poses a dilemma, of correlating two joint angles to three joint angles, should the mapping occur in joint space.

Recent years have witnessed a growing interest in freehand 3D human–machine interaction. Digits, a wrist-worn motion capture device that utilizes laser scan, show encouraging 3D spatial interaction with mobile devices and eyes-free interaction [54]. Leapfrog, a 80 mm long device that uses light-emitting diodes and small cameras, promises tracking all ten fingers up to 0.01 mm [55]. It would be fascinating to see these devices applied to teleoperating a robotic hand.

We addressed the problem of teleoperating a humanoid robotic thumb, enabling grasping objects with the index finger. Three-fingered hands, such as the King's College London Metamorphic Hand [17], are the mainstream end-effector in terms of cost and efficiency. Our future work will be using data gloves to teleoperate three-fingered hands and will be addressing one critical issue: measuring the palm movements and reflecting them on the relative positioning of the fingers.

8 Conclusions

We used a data glove as the input to teleoperate a humanoid robotic thumb, focusing on both the position and the orientation of the thumb fingertip—this differed from previous approaches that only considered fingertip position. We presented a novel human-thumb model that matched the data-glove-sensor positioning and developed an experimental protocol that required each operator to grasp a set of nine rigid objects with the index finger and thumb. Scrutinizing the initial mapping function reduced the number of parameters from 22 to 17, which were subsequently optimized by a nonlinear constrained-optimization technique. This approach required minimum extra hardware and the lengths of the rigid objects covered the graspable range by the index and thumb fingertips, ensuring the objects with intermediate length were also graspable. We further discussed various factors that affected the calibration accuracy.

Acknowledgment

The first author would like to thank Mr. Rich Walker for his insightful suggestions and Dr. Ketao Zhang for his assistance. The valuable comments to earlier versions of the article provided by three anonymous reviewers are also gratefully acknowledged.

References

[1] Goertz, R., 1964, "Manipulator Systems Development at ANL," 12th Conference on Remote Systems Technology, American Nuclear Society, San Francisco, CA, pp. 117–136.
[2] Zoppi, M., Sieklicki, W., and Molfino, R., 2008, "Design of a Microrobotic Wrist for Needle Laparoscopic Surgery," ASME J. Mech. Des., **130**(10), p. 102306.
[3] Li, J., Zhang, G., Müller, A., and Wang, S., 2013, "A Family of Remote Center of Motion Mechanisms Based on Intersecting Motion Planes," ASME J. Mech. Des., **135**(9), p. 091009.
[4] Kuo, C.-H., and Dai, J. S., 2012, "Kinematics of a Fully-Decoupled Remote Center-of-Motion Parallel Manipulator for Minimally Invasive Surgery," ASME J. Med. Dev., **6**(2), p. 021008.
[5] Dai, J. S., 2010, "Surgical Robotics and Its Development and Progress," Robotica, **28**(2), pp. 161–161.
[6] Verner, M., Xi, F., and Mechefske, C., 2005, "Optimal Calibration of Parallel Kinematic Machines," ASME J. Mech. Des., **127**(1), pp. 62–69.
[7] Safaric, R., Parkin, R. M., Czarnecki, C. A., and Calkin, D. W., 2001, "Virtual Environment for Telerobotics," Integr. Comput.-Aided Eng., **8**(2), pp. 95–104.
[8] Bi, Z. M., Lang, S. Y. T., Zhang, D., Orban, P. E., and Verner, M., 2006, "Integrated Design Toolbox for Tripod-Based Parallel Kinematic Machines," ASME J. Mech. Des., **129**(8), pp. 799–807.
[9] Bicchi, A., Caiti, A., Pallottino, L., and Tonietti, G., 2005, "Online Robotic Experiments for Tele-Education at the University of Pisa," J. Rob. Syst., **22**(4), pp. 217–230.
[10] Kihonge, J. N., Larochelle, P. M., and Vance, J. M., 2002, "Spatial Mechanism Design in Virtual Reality With Networking," ASME J. Mech. Des., **124**(3), pp. 435–440.
[11] Moosavian, S. A. A., Kalantari, A., Semsarilar, H., Aboosaeedan, E., and Mihankhah, E., 2009, "ResQuake: A Tele-Operative Rescue Robot," ASME J. Mech. Des., **131**(8), p. 081005.
[12] Springer, S. L., and Ferrier, N. J., 2002, "Design and Control of a Force-Reflecting Haptic Interface for Teleoperational Grasping," ASME J. Mech. Des., **124**(2), pp. 277–283.
[13] Snyman, J. A., Duffy, J., and du Plessis, L. J., 1998, "An Optimization Approach to the Determination of the Boundaries of Manipulator Workspaces," ASME J. Mech. Des., **122**(4), pp. 447–456.
[14] Rahman, T., Krouglicof, N., and Lye, L., 2012, "Kinematic Synthesis of Nonspherical Orientation Manipulators: Maximization of Dexterous Regular Workspace by Multiple Response Optimization," ASME J. Mech. Des., **134**(7), p. 071009.
[15] Gan, D., Tsagarakis, N. G., Dai, J. S., Caldwell, D. G., and Seneviratne, L., 2012, "Stiffness Design for a Spatial Three Degrees of Freedom Serial Compliant Manipulator Based on Impact Configuration Decomposition," J. Mech. Rob., **5**(1), p. 011002.
[16] Zhang, X., and Nelson, C. A., 2011, "Multiple-Criteria Kinematic Optimization for the Design of Spherical Serial Mechanisms Using Genetic Algorithms," ASME J. Mech. Des., **133**(1), p. 011005.
[17] Dai, J. S., Wang, D., and Cui, L., 2009, "Orientation and Workspace Analysis of the Multifingered Metamorphic Hand-Metahand," IEEE Trans. Rob., **25**(4), pp. 942–947.
[18] Cui, L., and Dai, J. S., 2011, "Posture, Workspace, and Manipulability of the Metamorphic Multifingered Hand With an Articulated Palm," ASME J. Mech. Rob., **3**(2), p. 021001.

[19] Cui, L., and Dai, J. S., 2012, "Reciprocity-Based Singular Value Decomposition for Inverse Kinematic Analysis of the Metamorphic Multifingered Hand," ASME J. Mech. Rob., **4**(3), p. 034502.
[20] Dai, J. S., and Wang, D., 2007, "Geometric Analysis and Synthesis of the Metamorphic Robotic Hand," ASME J. Mech. Des., **129**(11), pp. 1191–1197.
[21] Wei, G., Dai, J. S., Wang, S., and Luo, H., 2011, "Kinematic Analysis and Prototype of a Metamorphic Anthropromorphic Hand With a Reconfigurable Palm," Int. J. Humanoid Rob., **8**(3), pp. 459–479.
[22] Collins, C. L., and Long, G. L., 1995, "The Singularity Analysis of an In-Parallel Hand Controller for Force-Reflected Teleoperation," IEEE Trans. Rob. Autom., **11**(5), pp. 661–669.
[23] Zhang, K., Fang, Y., Dai, J. S., and Fang, H., 2010, "Geometry and Constraint Analysis of the Three-Spherical Kinematic Chain Based Parallel Mechanism," J. Mech. Rob., **2**(3), p. 031014.
[24] Dipietro, L., Sabatini, A. M., and Dario, P., 2008, "A Survey of Glove-Based Systems and Their Applications," IEEE Trans. Syst. Man Cybern. Part C, **38**(4), pp. 461–482.
[25] Fischer, M., van der Smagt, P., and Hirzinger, G., 1998, "Learning Techniques in a Dataglove Based Telemanipulation System for the DLR Hand," IEEE International Conference on Robotics and Automation, IEEE Press, Leuven, Belgium, pp. 1603–1608.
[26] Griffin, W. B., Findley, R. P., Turner, M. L., and Cutkosky, M. R., 2000, "Calibration and Mapping of a Human Hand for Dexterous Telemanipulation," ASME International Mechanical Engineering Congress, ASME Press, Orlando, FL, pp. 1–8.
[27] Rohling, R. N., and Hollerbach, J. M., 1993, "Calibrating the Human Hand for Haptic Interfaces," Presence, **2**(4), pp. 281–296.
[28] Hong, J., and Tan, X., 1989, "Calibrating a VPL DataGlove for Teleoperating the Utah/MIT Hand," IEEE International Conference on Robotics and Automation, IEEE Press, Scottsdale, AZ. pp. 1752–1757.
[29] Wojtara, T., Nonami, K., Shao, H., Yuasa, R., Amano, S., and Nobumoto, Y., 2004, "Master-Slave Hand System of Different Structures, Grasp Recognition by Neural Network and Grasp Mapping," Robotica, **22**(4), pp. 449–454.
[30] Chang, L. Y., and Pollard, N. S., 2007, "Constrained Least-Squares Optimization for Robust Estimation of Center of Rotation," J. Biomech., **40**(6), pp. 1392–1400.
[31] Chang, L. Y., and Pollard, N. S., 2007, "Robust Estimation of Dominant Axis of Rotation," J. Biomech., **40**(12), pp. 2707–2715.
[32] Diftler, M. A., Culbert, C. J., Ambrose, R. O., Platt, R., Jr., and Bluethmann, W. J., 2003, "Evolution of the NASA/DARPA Robonaut Control System," IEEE International Conference on Robotics and Automation, IEEE Press, Taipei, pp. 2543–2548.
[33] Napier, J., 1956, "The Prehensile Movements of the Human Hands," J. Bone Joint Surg., **38B**(4), pp. 902–913.
[34] Cutkosky, M. R., and Kao, I., 1989, "Computing and Controlling Compliance of a Robotic Hand," IEEE Trans. Rob. Autom., **5**(2), pp. 151–165.
[35] Cooney, W., and Chao, E., 1977, "Biomechanical Analysis of Static Forces in the Thumb During Hand Function," J. Bone Joint Surg., **59**(1), pp. 27–36.
[36] Taylor, C. L., and Schwarz, R. J., 1995, "The Anatomy and Mechanics of the Human Hand," Artif. Limbs, **2**(2), pp. 22–35.
[37] Dai, J. S., and Kerr, D. R., 1996, "Analysis of Force Distribution in Grasps Using Augmentation," Proc. Inst. Mech. Eng., Part C, **210**(1), pp. 15–22.
[38] Sanli, S. G., Kizilkanat, E. D., Boyan, N., Ozsahin, E. T., Bozkir, M. G., Soames, R., Erol, H., and Oguz, O., 2005, "Stature Estimation Based on Hand Length and Foot Length," Clin. Anatomy, **18**(8), pp. 589–596.
[39] Cupcic, U., 2013, "Shadow Robot's ROS Interface," https://launchpad.net/sr-ros-interface
[40] Santos, V. J., and Valero-Cuevas, F. J., 2006, "Reported Anatomical Variability Naturally Leads to Multimodal Distributions of Denavit-Hartenberg Parameters for the Human Thumb," IEEE Trans. Biomed. Eng., **53**(2), pp. 155–163.
[41] Virtual Technologies, 1992, *CyberGlove User's Manual*, Virtual Technologies, Oakland, MI.
[42] Cooney, M. P., Lucca, M. J., Chao, E. Y., and Linscheid, R. L., 1981, "The Kinesiology of the Thumb Trapeziometacarpal Joint," J. Bone Joint Surg., **63**(9), pp. 1371–1381.
[43] Hartenberg, R. S., and Denavit, J., 1964, *Kinematic Synthesis of Linkages*, McGraw-Hill, Inc., New York.
[44] Murray, R. M., Li, Z., and Sastry, S. S., 1994, *A Mathematical Introduction to Robotic Manipulation*, CRC Press, Boca Raton, FL.
[45] Li, H., Trinkle, J. C., and Li, Z. X., 2000, "Grasp Analysis as Linear Matrix Inequality Problems," IEEE Trans. Rob. Autom., **16**(6), pp. 663–674.
[46] Johnson, K. L., 1987, *Contact Mechanics*, Cambridge University Press, Cambridge, UK.
[47] Ghafoor, A., Dai, J. S., and Duffy, J., 2000, "Fine Motion Control Based on Constraint Criteria Under Pre-Loading Configurations," J. Rob. Syst., **17**(4), pp. 171–185.
[48] Bicchi, A., and Kumar, V., 2000, "Robotic Grasping and Contact: A Review," IEEE International Conference on Robotics and Automation, IEEE Press, San Francisco, pp. 348–353.
[49] Howard, W. S., and Kumar, V., 1996, "On the Stability of Grasped Objects," IEEE Trans. Rob. Autom., **12**(6), pp. 904–917.
[50] Dietrich, J., Hirzinger, G., and Heindl, J., 1999, *Multisensory Telerobotic Techniques*, Springer-Verlag, Berlin, Germany.
[51] Anil, S. M., Bobby, B., Rose, M., Cynthia, D. B., Er, T., Jeff, S., Kevin, M., and Richard, B., 2003, "Using Registration, Calibration, and Robotics to Build a More Accurate Virtual Reality Simulation for Astronaut Training and Telemedicine," International Conference on Computer Graphics and Computer Vaclav Skala Union Agency, Vision Plzen-Bory, Czech Republic.
[52] Ben-Haim, Z., and Eldar, Y. C., 2005, "Minimax Estimators Dominating the Least-Squares Estimator," IEEE International Conference on Acoustics, Speech, and Signal Processing, IEEE Press, Philadelphia, PA, Vol. 4, pp. 53–56.
[53] Schmidt, K., 1996, "A Comparison of Minimax and Least Squares Estimators in Linear Regression With Polyhedral Prior Information," Acta Appl. Math., **43**(1), pp. 127–138.
[54] Kim, D., Hilliges, O., Izadi, S., Butler, A. D., Chen, J., Oikonomidis, I., and Olivier, P., 2012, "Digits: Freehand 3D Interactions Anywhere Using a Wrist-Worn Gloveless Sensor," 25th Annual ACM Symposium on User Interface Software and Technology, ACM, Cambridge, MA, pp. 167–176.
[55] Leap Motion, 2013. Available at: https://www.leapmotion.com/product